IRON LOSSES EVALUATION IN HIGH SPEED DRIVES

G. D. Kalokiris[1], P. S. Georgilakis[2] and A. G. Kladas[1]

[1] National Technical University of Athens, GR-15780, Greece
(e-mail: kladasel@central.ntua.gr)

[2] Technical University of Crete, GR-73100, Chania, Greece
(e-mail: pgeorg@dpem.tuc.gr)

ABSTRACT

The paper presents electrical machine design considerations introduced by exploiting new magnetic material characteristics. The materials considered are amorphous alloy ribbons as well as Neodymium alloy permanent magnets involving very low eddy current losses. Such advance materials enable electric machine operation at higher frequencies compared with the standard iron laminations used in the traditional magnetic circuit construction and provide better efficiently.

Keywords: Finite element method, permanent magnets, rotor skew, design methodology.

1. INTRODUCTION

A methodology for electrical machine modeling enabling to exploit new magnetic material characteristics are presented by the authors. The materials considered are thin magnetic laminations, amorphous alloy ribbons as well as Neodymium alloy permanent magnets involving very low eddy current losses as mentioned in (1)-(3). Such materials enable electric machine operation at high frequencies compared with the standard iron laminations used in the traditional magnetic circuit construction. Moreover, simpler winding configurations are adopted, taking into consideration that there will be a power electronics converter ensuring the connection of the machine to the electric grid (4)-(6).

The study of asynchronous and permanent magnet machines based on such materials is undertaken in three steps. In a first step the typical design procedure is conveniently adapted in order to include the new magnetic material properties. In a second the designed machine characteristics are checked by means of a detailed field calculation through finite element modeling associated to sensitivity analysis techniques. In a third step a prototype is constructed in order to validate the machine performance. Low losses and high volumic power associated with high speed and converter machine operation are the main advantages of such applications (7)-(10).

2. CALCULATION METHODOLOGY

The proposed machine design procedure involves two steps. In a first step standard design methodology is used for preliminary design. In a second step the method of finite elements is implemented to calculate the machine efficiency and performance. Finally, prototypes are constructed in order to validate and compare the simulated machine characteristics to the corresponding experimental results (11)-(12).

In case of variable reluctance machines, the electromechanical conversion is based on the magnetic energy exchanges in the magnetic circuit with the variation of reluctance with rotor position and of excitation. In general, the stored energy in the magnetic circuit is maximized when the reluctance is minimum (conjunction) and is minimized when the reluctance is maximum (opposition), while the appropriate current variation ensures appropriate torque. The studied structure of machines is multidiscoidal (Fig. 1) with discs composed from non-magnetic resins where convenient ferromagnetic parts are embedded (1).

The method of finite elements, is based on a discretisation of the solution domain into small regions. In magnetostatic problems the unknown quantity is usually the magnetic vector potential A, and is approximated by means of polynomial shape functions. In two dimensional cases triangular elements can easily be adapted to complex configurations and first order elements exhibit advantages in iron saturation representation (13). The size of elements must be small enough to provide sufficient accuracy. In this way the differential equations of the continuous problem can be transformed into a system of algebraic equations for the discrete problem. The practical problems necessitate usually several tenths of thousands of unknowns.

However, appropriate numerical techniques have been developed, enabling to obtain the solution of such systems within reasonable time, even when personal computers are used. It should be mentioned that the 3D problems require considerably higher computational resources than the 2D ones. In the present paper the 2D finite element model adopted, involves vector potential formulation, while the magnetic flux Φ_m per pole can be calculated as follows:

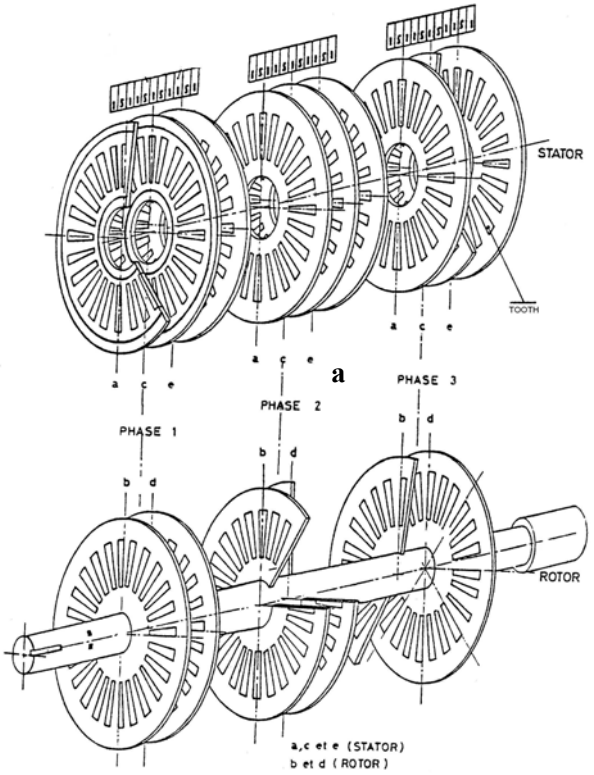

Figure 1. Multidiscoidal Variable Reluctance Machine structure studied.
a: stator part
b: rotor part

$$\Phi_m = \iint_{S_1} B \cdot dS = \oint_{C_1} A \cdot dl \cong \left(2\, A_{gap}\right) L_0 \qquad (1)$$

where L_0 is the length of the magnetic circuit in m, A is the magnetic vector potential, A_{gap} is the vector potential value in the middle of the air-gap, B is the flux density in Tesla, S_1 is the cross-sectional area normal to the direction of flux in m^2 and C_1 is the contour surrounding the surface S_1 in m. The electromotive force at no load can be calculated as follows:

$$E = -\frac{d\Phi_m}{dt} \qquad (2)$$

The value of the voltage of the machine operated as generator under load conditions can be calculated by relation (3):

$$V = E - RI - jL_\sigma \omega I \qquad (3)$$

where V is the voltage on stator windings in V, E is the electromotive force at no load in V, R is the stator resistance in Ω, L_σ is the stator leakage inductance in H, ω is the rotor angular velocity in rad/sec and I is the stator current in A. Then the magnetic flux and electromotive forces can be derived by using equations (1) and (2). Finally, we calculate the iron losses for this machine at the low and high frequency operation by the equation:

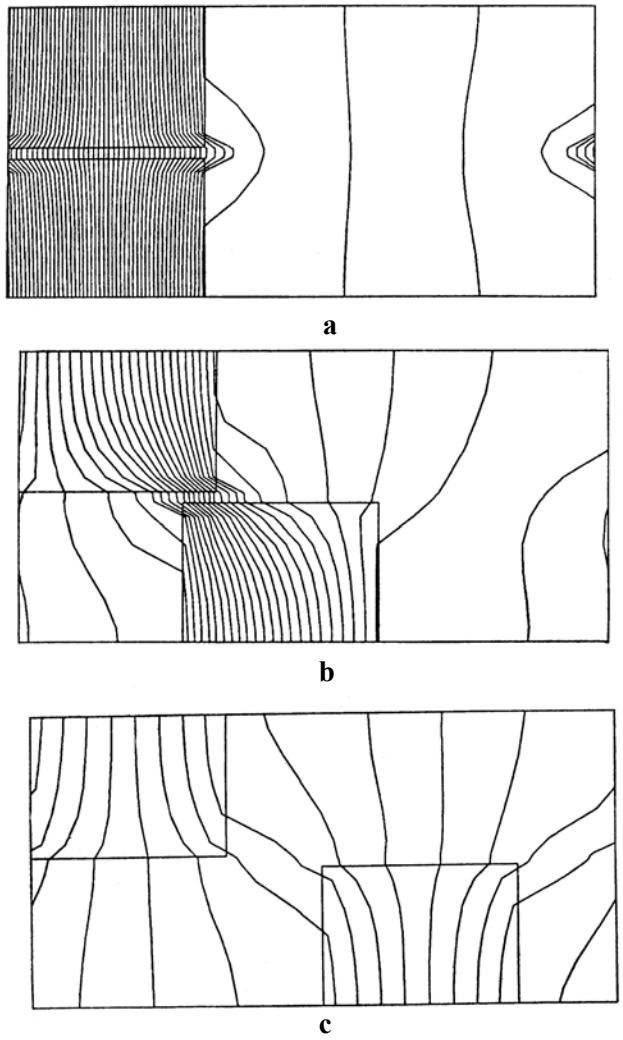

Figure 2. Flux distribution in the two dimensional variable reluctance machine configuration for low excitation.
a: Conjunction
b: Intermediate position
c: Opposition

$$P_{iron} = P_{total} - P_{Cu} \qquad (4)$$
$$\text{where } P_{Cu} = P_{Cu\ rotor} + P_{Cu\ stator}$$

3. RESULTS AND DISCUSSION

A. Variable Reluctance Machines

The variable reluctance machine considered is three phase comprising three stator discs and two rotor discs for each phase mounted on the same transaxle, as shown in Fig. 1. Each disc comprises 24 ferromagnetic teeth while each phase has appropriate flux return core parts.

The magnetic field analysis has been performed in two dimensional Cartesian approximation by considering a peripheral cutaway of the active part of the machine as shown in Fig.2. This figure shows the magnetic field density distribution for different rotor

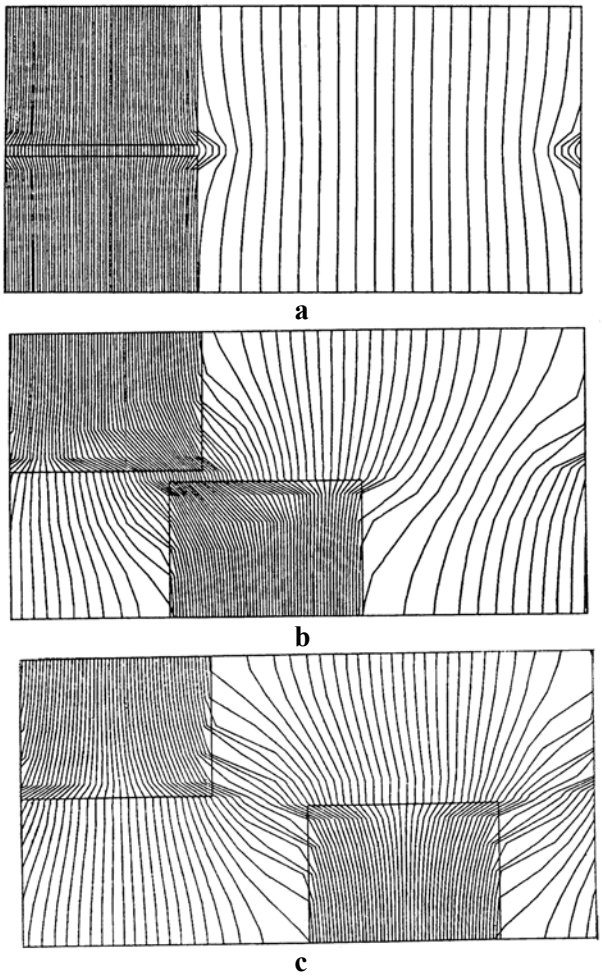

Figure 3. Flux distribution in the two dimensional variable reluctance machine configuration for high excitation.
a: Conjunction
b: Intermediate position
c: Opposition

positions in case of low excitation current. The magnetic circuit in this case is unsaturated. The same results for high excitation current are shown in Fig. 3. It may be noted that the teeth are highly saturated in this case, especially in the corners for intermediate positions (Fig. 3b).

The reduced torque per excitation can be calculated by convenient radial extrapolation of the two dimensional results and the obtained results are shown in Fig. 4. This figure compares the numerical (continuous line) results with the measured ones (dashed line). The two curves variations with rotor position are similar but the measured results are somewhat smaller due to the fact the return flux circuits (3D feature) has been neglected in the two dimensional representation.

An important part of losses in variable reluctance machines is due to hysterisis effect and in order to account for this an appropriate Preisach-Neel model has been developed for the iron laminations used (14).

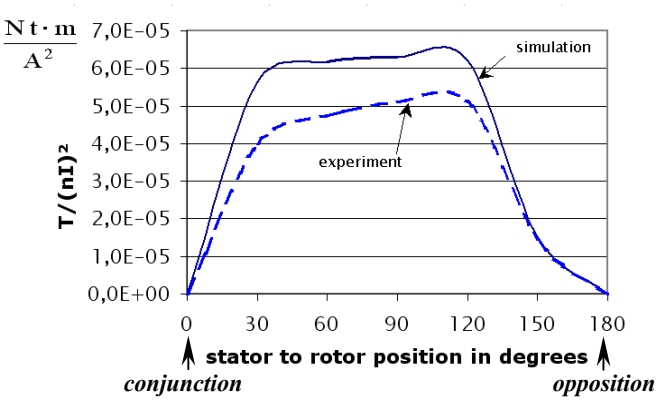

Figure 4. Reduced torque per excitation in the variable reluctance machine with rotor position.

In order to associate appropriate weights to this model the experimental hysterisis curves obtained for the iron laminations used have been considered, shown in Fig. 5.

In various points of the ferromagnetic teeth of the variable reluctance machine different hysterisis curves are obtained, which vary also with the excitation imposed. One characteristic of the machine tested, involving unidirectional excitation, is that minor hysterisis curves are obtained as shown in Figs. 6 and 7.

The calculated curves in these figures have been obtained by making two important assumptions: the field density values are computed through the two dimensional analysis presented (end magnetic circuit effects as well as return flux paths are neglected) while eddy currents in iron laminations was supposed to have negligible effects on local field value variations (static field analysis).

Moreover, the Preisach-Neel model adopted ignores frequency variation effects and assumes unidirectional flux density variations (rotational field effects are not accounted).

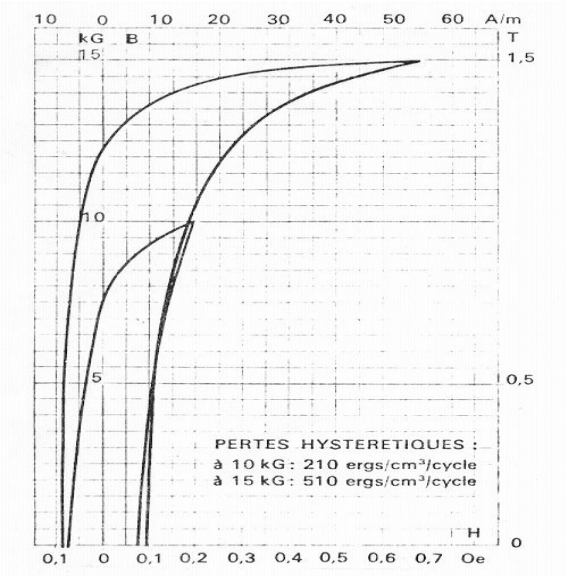

Figure 5. Experimental hysterisis curves obtained with direct current excitation for the 0.35 mm width iron laminations used.

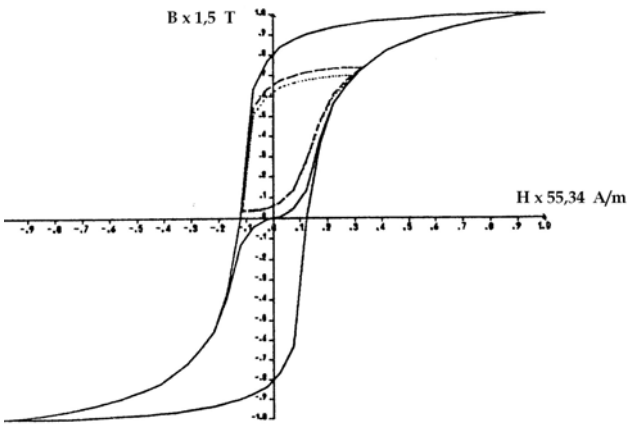

Figure 6. Unidirectional excitation of the variable reluctance machine and minor hysterisis curves calculated.

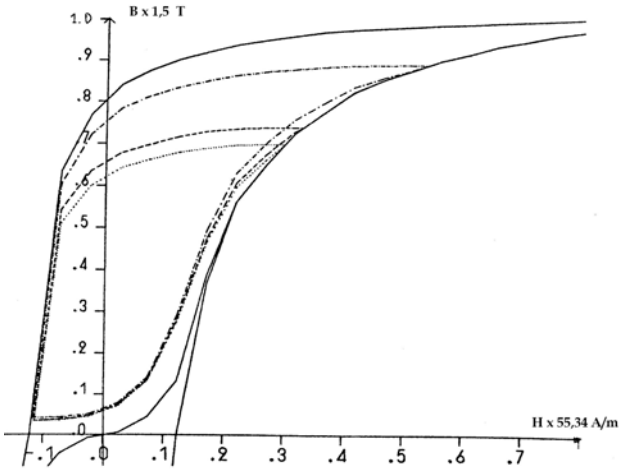

Figure 7. Minor hysterisis curves calculated in various points of the teeth of the variable reluctance machine.

B. Permanent Magnet Machines

The case of a permanent magnet machine has been considered. The machine designed has been checked through a 2.5 kW prototype which has been connected to an appropriate power electronics converter. The air-gap width has been chosen 1 mm while a multipole "peri-pheral" machine structure has been adopted. The geometry of the permanent magnet machine is given in (6) providing also the mesh employed for the two dimensional finite element program of the machine involving, approximately 2100 nodes 4000 triangular elements.

In a first step the no load operating conditions have been examined. The corresponding simulated voltage waveform is shown in Fig. 8 while the measured one is given in Fig. 9, respectively. In these figures a good agreement between the simulated and measured results can be observed. The simulation results concerning full load voltage of synchronous generator are presented in Fig. 10.

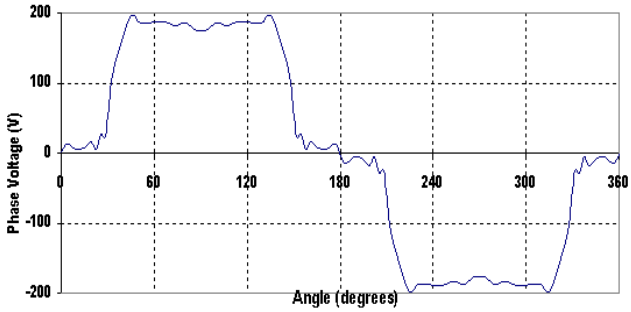

Figure 8. No load voltage waveform of permanent magnet machine (simulation)

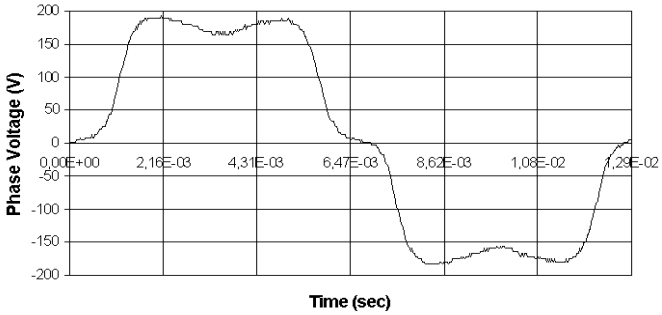

Figure 9. No load voltage waveform of permanent magnet machine (measurement)

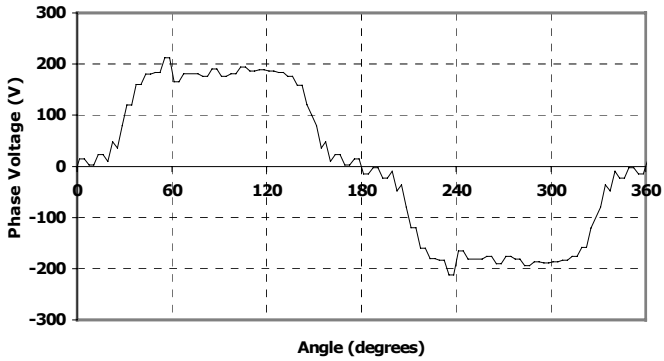

Figure 10. Full load voltage waveform of permanent magnet machine (simulation)

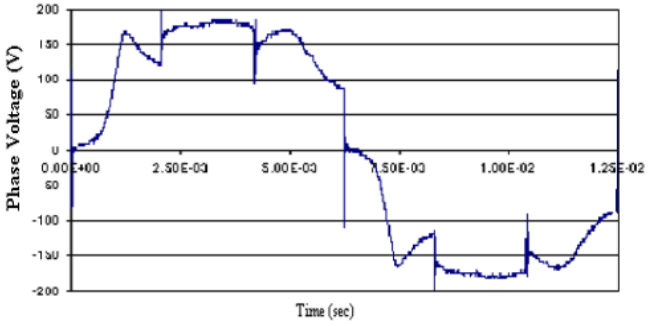

Figure 11. Full load voltage waveform of permanent magnet machine (measurement)

Figure 11 gives the measured results under the same operating conditions. A good agreement can be observed in these figures between the simulated and measured results also in the case of full load.

C. Asynchronous Machines

Moreover, measurements were realized for an asynchronous motor, which was supplied by an inverter with variable frequency. The motor is a three phase, 4-pole, machine supplied at a frequency of 400 Hz, at a voltage of 208 V while the nominal, speed is 10.800 rpm. The motor was tested under no load and low load operating conditions, for various frequencies. Fig. 12a shows the field distribution in the machine supplied at fundamental frequency of 300 Hz, while Fig. 12b gives the field distribution at the switching frequency of 10 kHz.

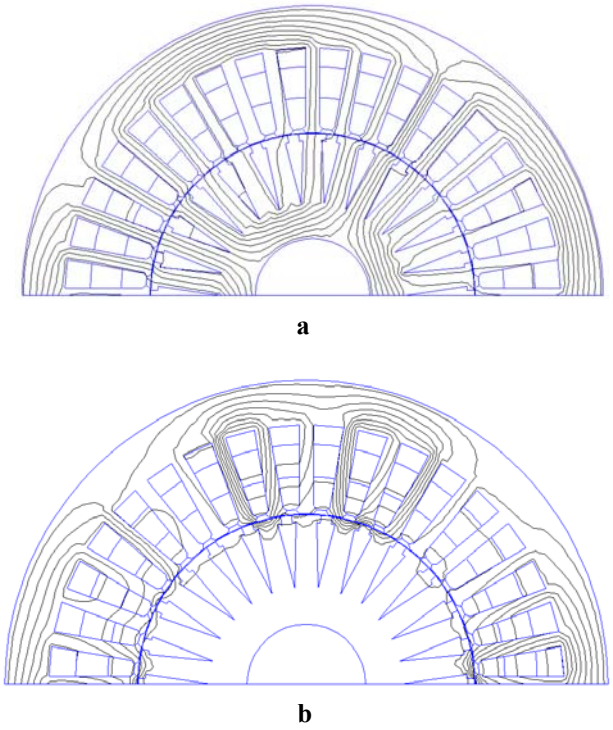

Figure 12. Simulated field distribution in the machine under low load conditions

a: fundamental supply frequency of 300Hz
b: switching frequency of 10 kHz

Fig. 13 presents the respective measured phase voltage and current time variations. Fig. 14 shows the field distribution in the machine supplied at fundamental frequency of 100 Hz, while Fig. 15 presents the respective measured phase voltage and current time variations at the switching frequency of 10 kHz. Table I presents the measured and simulation results under no load conditions with a switching frequency of 1 kHz. Table II presents the same results under low load conditions. Table III presents the results related to a switching frequency of 10 kHz. The simulated torque T_s is calculated by the relation:

$$T_s = F_t \cdot r_g \qquad (5)$$

where F_t is the total circumferential tangential force in Newton and r_g is the middle air-gap radius in meters. The Maxwell' s stress tensor is calculated by relation (6):

$$F_t = \frac{1}{\mu_0} \oint_C B_n \, B_t \, dl \, L_0 \qquad (6)$$

where B_n and B_t are the normal and tangential magnetic flux density components, respectively, to the integration surface of air-gap C in Tesla, μ_0 is the permeability of air and L_0 is the active part of the machine.

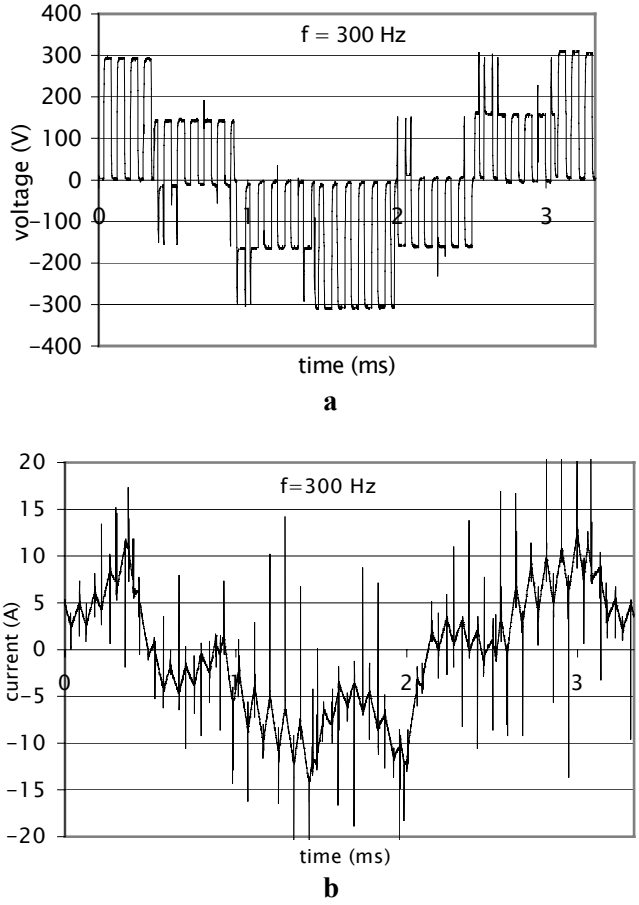

Figure 13. Measured supply quantities in the machine for supply frequency of 300 Hz, under low load conditions

a: phase voltage time variation
b: phase current time variation

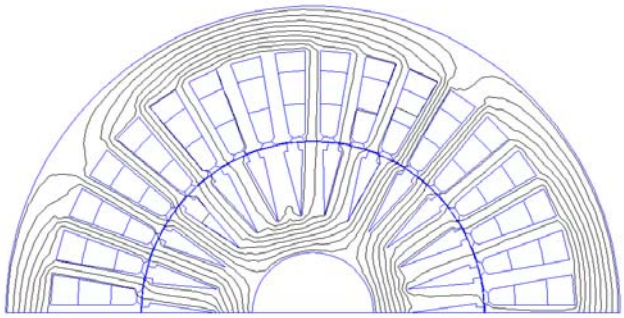

Figure 14. Simulated field distribution in the machine, fundamental supply frequency of 100 Hz under low-load conditions

In Tables I, II and III a good agreement between the measured and simulated results for both voltage and torque values can be observed.

Table I. Measured and simulation results under no load conditions and f_s= 1 kHz

f_s= 1 KHz no load					
$f_{1\ fundamental}$ (Hz)	$I_{1measured}$ (A)	$V_{1measured}$ (V)	$T_{measured}$ (Nt·m)	$V_{1simulated}$ (V)	$T_{simulated}$ (Nt·m)
20	1,587	4,717	0	2,041	0,055
50	2,267	14,350	0,1	13,279	0,088
75	2,417	20,962	0,15	21,096	0,11

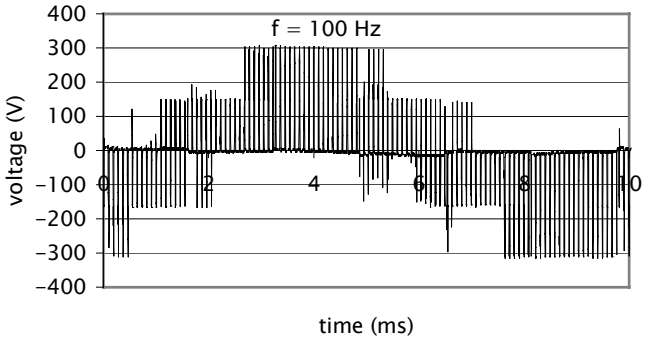

a

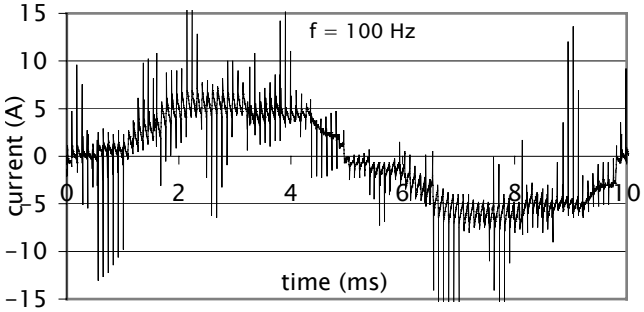

b

Figure 15. Measured supply quantities in the machine for supply frequency of 100 Hz under low load conditions

a: phase voltage time variation
b: phase current time variation

Table II. Measured and simulation results under low load conditions and f_s= 1 kHz

f_s= 1 KHz low load					
$f_{1\ fundamental}$ (Hz)	$I_{1measured}$ (A)	$V_{1measured}$ (V)	$T_{measured}$ (Nt·m)	$V_{1simulated}$ (V)	$T_{simulated}$ (Nt·m)
50	2,754	13,769	0,4	14,540	0,23

Table III. Measured and simulation results under low load conditions and f_s= 10 kHz

f_s= 10 KHz low load					
$f_{1\ fundamental}$ (Hz)	$I_{1measured}$ (A)	$V_{1measured}$ (V)	$T_{measured}$ (Nt·m)	$V_{1simulated}$ (V)	$T_{simulated}$ (Nt·m)
50	2,368	13,584	0,22	13,353	0,18
100	2,874	22,646	0,38	25,790	0,3
200	5,179	53,533	1,05	75,970	1,03

4. CONCLUSIONS

In this paper, methodologies are proposed in order to evaluate the iron losses in various types of electrical machines favored for high speed drive applications. Electrical machine operation has been investigated by using the finite element method for the machine analysis and verified by measurements. Moreover, the low cost involved makes such drives attractive rivals of the conventional ones.

5. REFERENCES

1. A. Kladas, “Etude du couple et des pertes fer d’une machine a reluctance variable”, report DEA, Universites Paris VI and Paris XI, 1983.
2. C. Marchand, Z. Ren, Z. and A. Razek, “Torque optimization of a buried permanent magnet synchronous machine by geometric modification using FEM”, in Proceedings EMF’94, Leuven, pp. 53-56, 1994.
3. A. Toba, T. Lipo, "Generic torque maximizing design methodology of surface permanent magnet Vernier machine", IEEE Trans. on Ind. Appl., Vol. 36, no 6, pp. 1539-1546, 2000.
4. G. Tsekouras, S. Kiartzis, A. Kladas, J. Tegopoulos, "Neural Network Approach compared to Sensitivity Analysis based on Finite Element Technique for Optimization of Permanent Magnet Generators", IEEE Trans. Magn., Vol. 37, no 5/1, pp. 3618-3621, 2001.
5. M. A. Alhamadi, N. Demerdash "Modeling and experimental verification of the performance of a skew mounted permanent magnet brushless dc motor drive with parameters computed from 3D FE magnetic field solutions", IEEE Trans. on Energy Conversion, Vol. 9, no 1, pp. 1-35, 1994.
6. G. D. Kalokiris, A. G. Kladas: "New magnetic material impact in electric machine design: high speed operation and reduction of losses", Journal of Sensors and Actuators A: Physical (Elsevier), vol.106, no 1/3, pp. 292-297.
7. G. D. Kalokiris, A. G. Kladas, J. A. Tegopoulos: "Permanent Magnet Machine Optimization by using FEM and Sensitivity Analysis Techniques", Optimisation and Inverse Problems in Electromagnetism, Kluwer Academic Publishers, pp. 287-294, ISBN 1-4020-1056-2.
8. G. D. Kalokiris, A. G. Kladas, J. A. Tegopoulos: “2D and 3D finite element design of skewed mounted permanent magnet synchronous generators”, Proceedings of the 3rd Japanese-Mediterranean Workshop on Applied Electromagnetic Engineering for Magnetic and Superconducting Materials”, accepted for publication in the Journal of Material Processing Technology, Elsevier.
9. M.R. Dubois, H. Polinder, and J.A. Ferreira, "Contribution of Permanent-Magnet Volume Elements to No-Load Voltage in Machines", IEEE Transactions on Magnetics, vol. 39/3, 2003, pp. 1784-1792.
10. P. Dziwniel, B. Boualem, F. Piriou, J.P. Ducreux, and P. Thomas "Comparison between two Approaches to Model Induction Machines with Skewed Slots", IEEE Transactions on Magnetics, vol. 36/4, 2000, pp. 1453-1457.
11. G. D. Kalokiris, Th. Kefalas, A. G. Kladas: “Special air-gap element for 2D FEM analysis of electrical machines accounting for rotor skew”, Eleventh Biennial IEEE Conference on Electromagnetic Field Computation (CEFC 2004), Seoul, Korea, June 6-9, 2004, pp. 357.
12. G.D. Kalokiris, A.G. Kladas: ”High speed machines using advanced magnetic materials analyzed by appropriate finite element models”, IASME Transactions, Vol. 1, no 2, April 2004, pp. 355-359.
13. H. De Gersem, K. Hameyer, T. Weiland, **"**Skew interface conditions in 2-D finite-element machine models**",** IEEE Transactions on Magnetics, vol.39/3, 2003, pp. 1452-1455.
14. G. Friedman, I.D. Mayergoyz, “Hysteretic energy losses in media described by vector Preisach model”, IEEE Transactions on Magnetics, Vol. 34 , no 4, pp. 1270-1272, July 1998.